(will be inserted by hand later)

Your thesaurus codes are:
01 (02.01.4; 08.01.1; 08.01.2; 08.03.5; 08.09.2 Capella; 13.25.5)

ASTRONOMY AND ASTROPHYSICS
September 30, 2000

The *XMM-Newton* view of stellar coronae: High-resolution X-ray spectroscopy of Capella*

M. Audard[1], E. Behar[2], M. Güdel[1], A.J.J. Raassen[3], D. Porquet[4], R. Mewe[3], C.A. Foley[5], and G.E. Bromage[6]

[1] Paul Scherrer Institut, Würenlingen and Villigen, 5232 Villigen PSI, Switzerland, e-mail: audard,guedel@astro.phys.ethz.ch
[2] Columbia Astrophysics Laboratory, Columbia University, New York, NY 10027, USA, e-mail: behar@astro.columbia.edu
[3] SRON Laboratory for Space Research, Sorbonnelaan 2, 3584 CA Utrecht, The Netherlands, e-mail: A.J.J.Raassen,R.Mewe@sron.nl
[4] CEA/DSM/DAPNIA, Service d'Astrophysique, CEA Saclay, F-91191 Gif-sur-Yvette Cedex, France, e-mail: dporquet@cea.fr
[5] Mullard Space Science Lab, University College London, Surrey, RH5 6NT, United Kingdom e-mail: caf@mssl.ucl.ac.uk
[6] Centre for Astrophysics, University of Central Lancashire, Preston PR1 2HE, United Kingdom, e-mail: g.e.bromage@uclan.ac.uk

Received September 30, 2000; accepted ??, 2000

Abstract. We present the high-resolution RGS spectrum of the bright stellar binary Capella observed by the *XMM-Newton* satellite. A multi-thermal approach has been applied to fit the data and derive elemental abundances. The differential emission measure distribution is reconstructed using a Chebychev polynomial fit. The DEM shape is found to display a sharp peak around 7 MK, consistent with previous *EUVE* and *ASCA* results. A small but significant amount of emission measure is required around 1.8 MK in order to explain the O VII He-like triplet and the C VI Lyα line. Using the sensitivity to temperature of dielectronic recombination lines from O VI around 22 Å, we confirm that the cool plasma temperature needs to be higher than 1.2 MK. In the approximation of a cool plasma described by one temperature, we used line ratios from the forbidden, intercombination, and resonance lines of the O VII triplet and derived an average density for the cool coronal plasma at the low density limit. A tentative study of line ratios from the Mg XI triplet gives an average temperature close to the sharp peak in emission measure and an average density of the order of 10^{12} cm^{-3}, three orders of magnitude higher than for O VII. Implications for the coronal physics of Capella are discussed. We complement this paper with a discussion of the importance of the atomic code uncertainties on the spectral fitting procedure.

Key words: atomic processes – stars: abundances – stars: activity – stars: coronae – stars: individual: Capella – X-rays: stars

1. Introduction

Bright X-ray coronal sources are ideal benchmarks for atomic codes. The Sun, the nearest coronal source, has extensively been used for this purpose (e.g., Phillips et al. 1999). Additional laboratory measurements such as with Electron Beam Ion Traps (EBIT; e.g., Brown et al. 1998) provide crucial additional information and constraints to atomic codes such as HULLAC (e.g., Bar-Shalom et al. 1998), MEKAL (Mewe et al. 1995), etc. However, neither the temperature structure of the X-ray Sun, nor the single-energy beams of laboratory experiments allow for a coverage of the full range of plasma temperatures and densities needed to understand cosmic X-ray sources. Stellar coronae, with their various levels of activity, differential emission measure distributions and densities, are natural and complementary benchmarks to atomic codes. Because of the small effective areas and low spectral resolution of previous X-ray instruments, it has been difficult to disentangle calibration uncertainties from incomplete atomic codes. The advent of new X-ray observatories such as *XMM-Newton* and *Chandra* allows us now to resolve and identify X-ray atomic transition lines. The high steady X-ray flux of Capella makes it one of the best candidates to study atomic physics.

2. Previous knowledge on Capella

Capella (α Aurigae; HD 34029; HR 1708; 13 Aurigae) is, at a distance of 12.93 pc (Perryman et al. 1997), one of the brightest optical and X-ray objects visible in the sky. It is composed of a G1 III and a G8 III star (Strassmeier & Fekel 1990, Hummel et al. 1994) separated by 56.47 mas (Hummel et al. 1994). The orbital period (P = 104 d) is not linked to the rotation period of each component, the G1 giant completing about 12 revolutions in one orbital period (Hummel et al. 1994). Catura et al. (1975) first detected weak X-ray emission from Capella, quickly confirmed by Mewe et al. (1975). Subsequent X-ray observations have been prolific with most X-ray satellites (Cash et al. 1978, Holt et al. 1979, Mewe et al. 1982, Vedder & Canizares 1983, Lemen et al. 1989, Dupree et al. 1993, Schrijver et al. 1995, Favata et al. 1997, Brickhouse et al. 2000, Brinkman et al. 2000, Canizares et al. 2000), however still leaving unresolved problems in the interpretation of Capella's coronal spectrum.

Send offprint requests to: M. Audard, audard@astro.phys.ethz.ch

* Based on observations obtained with XMM-Newton, an ESA science mission with instruments and contributions directly funded by ESA Member States and the USA (NASA)

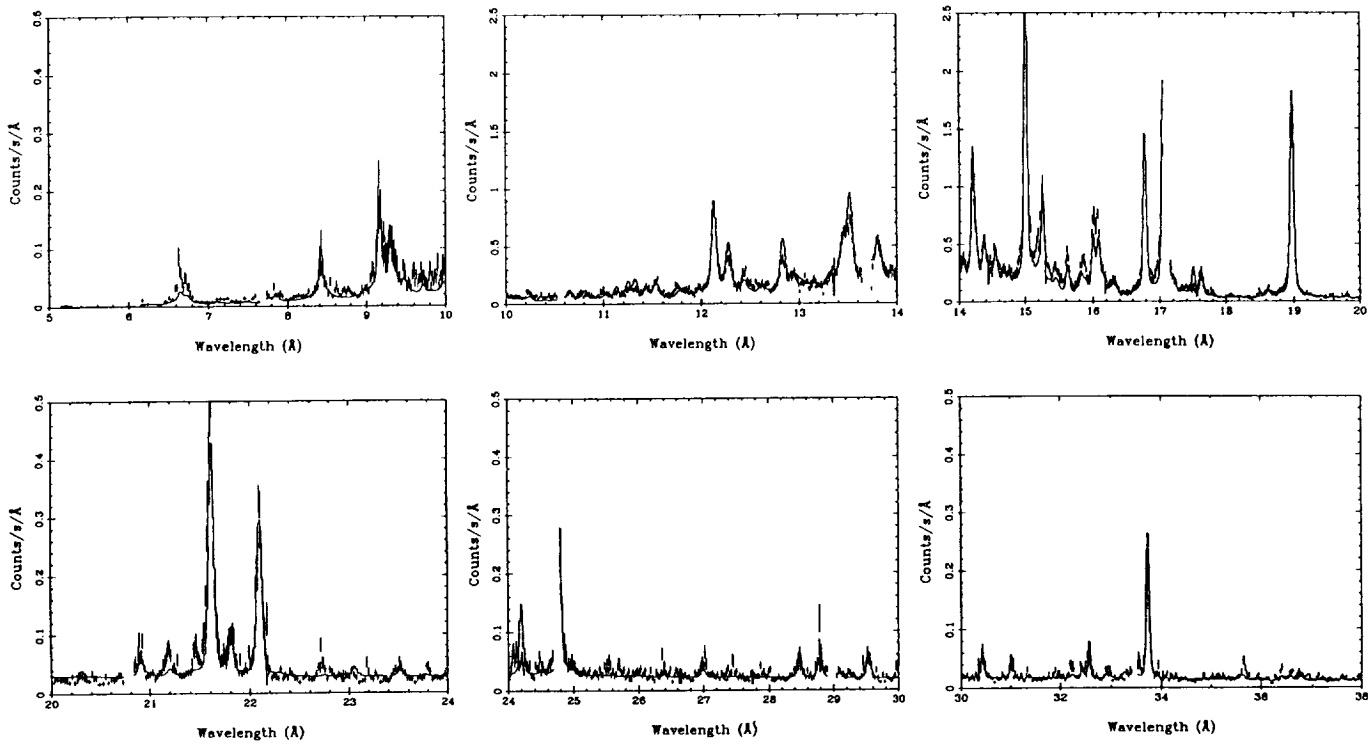

Fig. 1. RGS1 data with the overlaid model derived from a reconstructed differential emission measure distribution (Fig. 2).

Linsky et al. (1998) found that the contribution of both stars to the total flux of the coronal Fe XXI line in the ultraviolet regime was similar. Dupree et al. (1993) showed that iron (Fe XV-XXIV) was dominating the *Extreme Ultraviolet Explorer* (*EUVE*) spectrum. Their reconstructed differential emission measure distribution (DEM) ranged from 0.1 MK to 63 MK, with minimum emission measure around 1 MK and a sharp peak around 6 MK. Based on lines of highly ionized Fe XXI, they derived an electron density of $4 \times 10^{11} - 10^{13}$ cm^{-3}. However, their DEM could not reproduce satisfactorily later *BeppoSAX* results (Favata et al. 1997). In a very thorough analysis, Brickhouse et al. (2000) studied simultaneous *EUVE* and *ASCA* observations of Capella. Their *ASCA* data could not be well fitted by the *EUVE*-derived models, nor by the available plasma spectral emission models, therefore they carefully studied instrumental and atomic code effects on the fit procedure. Missing high-energy lines of Fe L-shell ions around 10 Å were proposed to explain the discrepancy between the best-fit model and their *ASCA* data. Brickhouse et al. (2000) also showed that the EUV intensities of Fe XXI to Fe XXIV vary by up to a factor of 4. They found that the low first-ionization-potential (FIP) elements Mg, Si, S, and Fe have coronal abundances consistent with solar photospheric values, while the high-FIP element Ne appears to be underabundant by a factor of 3 to 4. However, they were not able to constrain the O abundance.

Recent first results on Capella were obtained from *Chandra* HETG/LETG (Behar et al. 2000, Brinkman et al. 2000, Canizares et al. 2000, Mewe et al. 2000b, Ness et al. 2000), confirming the dominance of Fe lines in the emission line spectrum of Capella. Density diagnostics applied to the C V, N VI and O VII triplets implied a low density regime ($1.5 - 9 \times 10^9$ cm^{-3} for LETG data, $0.8 - 2 \times 10^{10}$ cm^{-3} for HETG data), while the hot Mg XI and Si XIII triplets give upper limits near 7×10^{11} and 1×10^{12} cm^{-3} in HETG. Little (or no) evidence for opacity effects in the 15.014 Å Fe XVII line has been seen (Brinkman et al. 2000). In a study of the X-ray line spectrum of the HETG data, Behar et al. (2000) showed that the Fe L-shell spectrum could be fairly well reproduced by assuming a single electron temperature of 0.6 keV. The present paper intends to present first results from the observation of Capella with *XMM-Newton*.

3. Data reduction

Capella was observed several times by *XMM-Newton* (Jansen et al. 2000, this issue) for calibration purposes. The *XMM-Newton* satellite carries 5 X-ray detectors and an optical telescope: two MOS European Photon Imaging Cameras (EPIC; Turner et al. 2000, this issue), one EPIC pn (Strüder et al. 2000, this issue), two Reflection Grating Spectrometers (RGS; den Herder et al. 2000, this issue) and an Optical Monitor (Mason et al. 2000, this issue).

In this paper, we present results of the on-axis observation (revolution 54, 2000-03-25, 11:36:59 UT until 2000-03-26, 02:53:49 UT) which had a low instrumental background. The effective exposures were 52.3 and 52.4 ksec for RGS1 and RGS2, respectively. No EPIC data is available due to the high

Table 1. Line fluxes in 10^{-4} s^{-1} cm^{-2}

Ion	λ (Å)	RGS1[a]	RGS2[a]	RGS1[b]	RGS2[b]	HETG[c]	HETG[d]	LETG[e]
Fe XVII	15.014	34.1	39.7	31.7	31.1	30.0	30.4	34.1
Fe XVII	16.775	19.8	22.5	18.8	19.5	20.9	20.0	20.4
Fe XVII	17.051		25.9		26.4	25.2	26.4	30.9
Fe XVII	17.100		30.7		25.8	24.3	24.4	24.4
O VIII	18.969	22.9	26.8	20.6	24.4		26.3	26.4
O VII	21.602	7.6		7.39			9.7	9.9
O VII	21.804	1.1		1.24			2.6	1.9
O VII	22.101	4.8		4.85			7.4	6.9
N VII	24.781		6.3		5.6		5.5	6.9
C VI	33.734	7.1	7.9	6.11				8.7

[a] LSF method, [b] Parametric method
[c] Behar et al. (2000), [d] Canizares et al. (2000), [e] Mewe et al. (2000b)

level of optical contamination and pile-up. The OM was closed because of the optical brightness of Capella.

The data were analyzed with the core XMM Science Analysis System (SAS[1]) software, version 4.1, and an update of several RGS tasks together with the latest current calibration files available at the time of the analysis. The metatask RGSPROC 0.77 was used to process the RGS data. Normally, the dispersion angles can be corrected for attitude drifts during the exposure. However, since the full attitude information was not available for these early observations, no correction was applied. During the observation, a short 600 sec deviation in pointing (due to a single event upset) occurred, however without significant influence on the high S/N RGS spectra. Spectra were extracted along the dispersion direction using a spatial mask together with a cut in the dispersion-PI plane. The RGS response matrices were generated by RGSRMFGEN 0.29.

4. Results and Discussion

We have fitted the quiescent RGS spectra with three collisional ionization equilibrium (CIE) models in the Utrecht software SPEX 2.0 (Kaastra et al. 1996). A fourth CIE model was suggested by the χ^2 procedure, however the temperature was unconstrained and produced a featureless continuum. We believe that the incompleteness of the atomic code available in SPEX is the cause of such a very hot component: some lines are not reproduced correctly by our model. It follows that the overlap of wings of these lines produces a pseudo-continuum that tends to be erroneously interpreted by the fit procedure as a physical continuum component.

4.1. Line fluxes

A number of individual line fluxes have been measured in both RGS instruments (Table 1). First, a constant "background" level was adjusted in order to account for the real continuum or for the pseudo-continuum created by the overlap of several weak or neglected lines. Especially in the 9–18 Å region, the overlap of the line wings (originating from the instrumental line spread function, LSF) created an important pseudo-continuum. We then used two different approaches to describe the line profiles in order to derive the integrated line fluxes. The first method used the instrumental LSF, while the second method used a parametric formula of the kind $p_4(1 + [(x - p_1)/p_2]^2)^{-p_3}$, where p_1 is the centroid of the line, p_2 is its half width at half maximum, p_3 is an arbitrary power value, and p_4 is the normalization factor.

The current state of the RGS1 LSF underestimates the line fluxes (and profile width). Some of the lines were cut by bad columns or gaps. We only give the "uncorrupted" line fluxes. For comparison, we also give line fluxes as measured by *Chandra* HETG (Behar et al. 2000, Canizares et al. 2000) and LETG (Mewe et al. 2000b). Within the instrumental and calibration uncertainties, the RGS fluxes are similar to the non-simultaneous *Chandra* fluxes. Our parametric method yields better agreement with previous works than the instrumental LSF. There might be some indications for higher values in LETG for lower stages of ionization. This might suggest that the low temperature plasma has lower EM during the *XMM-Newton* observation. This is, however, opposite to the suggestion of Brickhouse et al. (2000) who found flux variations in the *hot* plasma component.

4.2. Abundances and Temperatures

In Table 2, we provide the best-fit parameters for both RGS1 and RGS2 spectra. The column density was fixed to 1.8×10^{18} cm^{-2} (Linsky et al. 1993). Abundances are given relative to the solar photospheric values. Figure 1 shows the RGS1 data with an overlaid best-fit model using a DEM distribution (see Fig. 2). The discrepancy of the fitting results between the two instruments is easily explained: among the two RGS, the RGS2 provides, at the time of writing, the superior calibration of the LSF. The 90 % confidence ranges for a single parameter are therefore only lower limits. In general, there is a good agreement between RGS1 and RGS2, although several values (notably Ne, Mg, Fe, Ni) reveal systematic deviations beyond the given errors. The Capella spectrum offers unprecedented

[1] http://xmm.vilspa.esa.es/sas/

Table 2. Best fits for the 3-T CIE model with 90 % confidence ranges.

Parameter	RGS1[a]	RGS2[a]
$\log N_{\rm H}$ [cm^{-2}]	$= 18.255$	$= 18.255$
kT_1 [keV]	$0.159^{+0.006}_{-0.006}$	$0.13^{+0.01}_{-0.01}$
kT_2 [keV]	$0.593^{+0.002}_{-0.002}$	$0.58^{+0.003}_{-0.004}$
kT_3 [keV]	$1.14^{+0.07}_{-0.07}$	$0.93^{+0.07}_{-0.07}$
$\log {\rm EM}_1$ [cm^{-3}]	$51.90^{+0.03}_{-0.02}$	$51.65^{+0.08}_{-0.09}$
$\log {\rm EM}_2$ [cm^{-3}]	$52.86^{+0.009}_{-0.01}$	$52.98^{+0.01}_{-0.01}$
$\log {\rm EM}_3$ [cm^{-3}]	$51.81^{+0.05}_{-0.05}$	$51.85^{+0.08}_{-0.09}$
C	$0.50^{+0.04}_{-0.04}$	$0.52^{+0.04}_{-0.04}$
N	$0.82^{+0.07}_{-0.07}$	$1.01^{+0.08}_{-0.08}$
O	$0.44^{+0.02}_{-0.01}$	$0.39^{+0.01}_{-0.01}$
Ne	$0.51^{+0.03}_{-0.03}$	$0.34^{+0.02}_{-0.02}$
Mg	$1.13^{+0.06}_{-0.05}$	$0.74^{+0.04}_{-0.04}$
Si	$0.41^{+0.06}_{-0.06}$	$0.48^{+0.06}_{-0.06}$
S	$0.14^{+0.02}_{-0.02}$	$0.09^{+0.02}_{-0.02}$
Ar	$0.23^{+0.1}_{-0.1}$	$0.17^{+0.14}_{-0.14}$
Ca	$0.27^{+0.08}_{-0.08}$	$0.27^{+0.11}_{-0.11}$
Fe	$0.62^{+0.02}_{-0.01}$	$0.51^{+0.01}_{-0.01}$
Ni	$0.88^{+0.07}_{-0.07}$	$0.54^{+0.05}_{-0.05}$

[a]The LSF calibration for RGS2 is better than for RGS1 at this time.

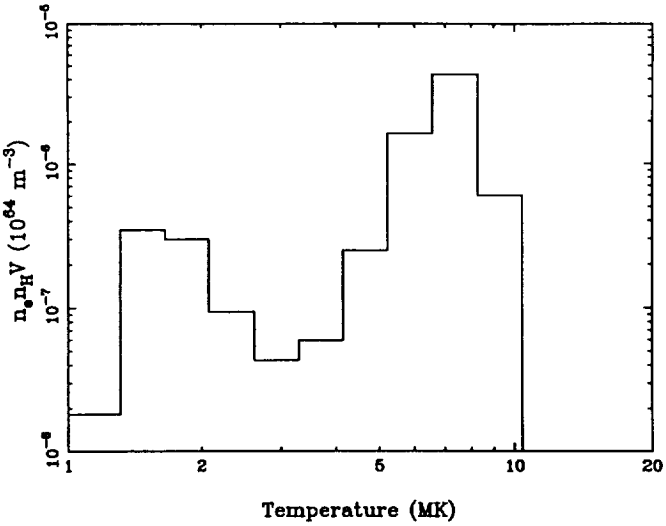

Fig. 2. Realization of a DEM for RGS1 data using Chebychev polynomials of order 5. The DEM does not show any EM above 10 MK.

S/N to investigate deficiencies in the present codes. The most important discrepancies occur for the Si XIII lines at 6.6 Å, for the high charge states of Fe XX–XXIV lines at 11.0 – 11.4 Å and at 12.8 Å, and for the Fe XVIII lines around 16 Å. Additionally, it can be noticed that the code fails to pick up some of the weak lines observed in the long-wavelength part of the spectrum, for example, the peaks around 35.7 (Ar XVI), 32.2 (Ar XVI), 27.5 (S XIII), 22.7 (Ca XV), 21.45 (Ca XVI), 21.2 (Ca XVII). HULLAC calculations indicate that these should mostly be attributed to L-shell emission from Si, S, Ar, and Ca.

We have iteratively eliminated emission lines and parts of the continuum that showed poor fit results, thus moving from global fitting towards a "single line analysis" approach. As an aside, we note here that the overlapping line wings as well as several line blends in the present RGS spectrum introduce considerable uncertainty if single line fluxes in the Fe L shell region are measured without modeling; we therefore kept the "global" approach for this test, even when eventually only a few bright line systems contributed to the results. The most important lines thus to eliminate were: Fe XVIII λ 16.0, O VIII Lyβ λ 16.0, Fe XVII and Fe XVIII lines at 15.4–15.8 Å, Fe XV, Fe XVI, O VI, and O VII lines between 17.4–17.6 Å, Fe XIX lines next to the Ne IX He-like triplet at 13.4–13.7 Å. As mentioned by Behar et al. (2000), the Fe XVIII lines around 16 Å are unexpectedly intense. They argued that two-step resonant excitation processes could explain the high intensity. Indeed, these processes, which consist of dielectronic capture followed by autoionization to a $2p^4 3s$ excited level, can considerably enhance these lines. The rates for these processes are, however, not yet available in the literature. Further weak lines of Fe XVII, Fe XVIII, Fe XIX, Fe XXI were removed as well. Despite the large reduction of the spectral information, the abundances turned out to be astonishingly robust. In all test runs, the Fe abundance was confined to within 0.50–0.68 (times solar photospheric), O within 0.24–0.39, and Ne within 0.75–1.05.

The S abundance is mostly influenced by the S XIV line at 24.2 Å in the model that is not nearly as strong in the data. By removing this line, we have determined an abundance of $0.35^{+0.04}_{-0.04}$ in both RGS. The weak S lines longwards to the S XIV line are somehow better fitted. Again, this is due to the incompleteness of the L-shell ions in our code. Similarly, by removing L-shell Si ions (in the long wavelength band), the bright Si He-like triplet is correctly fitted, with an abundance of 0.66 times the solar photospheric value.

Although we are aware that global fitting techniques strongly depend on the completeness and accuracy of presently available atomic codes, the results appear to show that such deficiencies are not likely to invalidate global fitting results as commonly used with low-resolution devices.

4.3. Differential emission measure distribution

The differential emission measure distribution of Capella that best represents the RGS spectrum has been reconstructed using the Chebychev polynomial fit approach as provided by SPEX. Figure 2 shows one realization of the DEM using a polynomial of order 5. No EM above 10 MK is needed for this realization. A sharp peak around 7 MK dominates the spectral emission lines, similar to previous (Dupree et al. 1993, Brickhouse et al. 2000) and recent *Chandra* results (Behar et al. 2000). However, the approximate upper envelope to the true EM distribution found by Canizares et al. (2000) does not reproduce the sharp peak, but indicates a broad distribution of temperature. It is possible that their assumption of solar abundances explains the discrepancy. However, we note that our DEM bears similar-

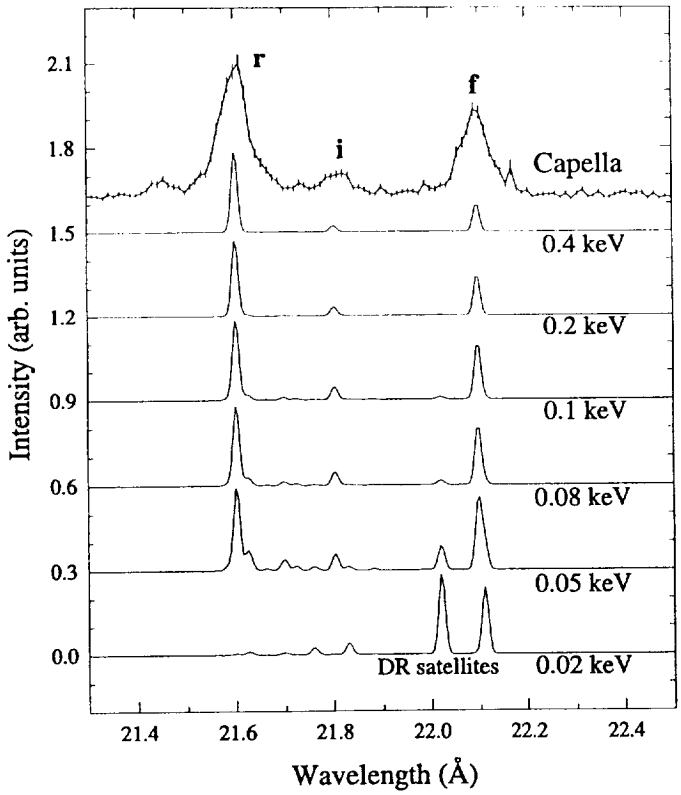

Fig. 3. Observed O VII triplet with calculated spectra of the O VII and O VI DR satellite lines for six different electron temperatures. The plots are normalized to the strongest line in each spectrum. Note the high temperature sensitivity of the DR satellites (see text).

ity to the DEM derived by Mewe et al. (2000b) with *Chandra* LETG data.

4.4. He-like ions

He-like ions emit three main lines, the so-called helium-like "triplet" lines: the resonance line (r), the intercombination line (i) and the forbidden line (f) (e.g., Gabriel & Jordan 1969, Pradhan 1982). For a single temperature plasma, the ratio $R{=}f/i$ and $G{=}(i+f)/r$ can be used to derive the electron density n_e and the electron temperature T_e.

In stellar coronae, continuous distributions in temperature of emission measure best describe the average coronal plasma. Indeed, a number of active regions, quiescent emission and flares are believed to exist simultaneously on active stars, in analogy with the Sun. We also recall that Capella is composed of two giant stars that are thought to produce a similar amount of coronal emission (Linsky et al. 1998). Therefore, any derivation of an electron density should be considered as a *weighted average* of the densities in the various regions of both coronae.

In this paper, we derive an average density from the O triplet around 22 Å and give a tentative result from the Mg triplet around 9.2 Å. The Si triplet is strongly blended because of the decreasing spectral resolution of the RGS at short wavelengths, while the Ne triplet is heavily blended by Fe and Ni lines. For the N VI, the line intensities were not unambigously determined. Based on the line fluxes from RGS1 data (the triplet is not avalaible for RGS2, see den Herder et al. 2000) using the parametric method, we derive from the O VII triplet, $R_{\rm obs} = 3.91$ and $G_{\rm obs} = 0.82$. For the Mg triplet, our tentative fluxes are 2.73, 0.81, and 1.56×10^{-4} s^{-1} cm^{-2} for the r, i, and f lines, respectively, hence $R_{\rm obs} = 1.93$ and $G_{\rm obs} = 0.87$. To derive the average formation temperature and density, we used theoretical calculations (Mewe et al. 2000a) that take into account the radiative and dielectronic recombinations, and the electronic collisional excitations (see Porquet & Dubau 2000 for the atomic data); they also take into account the influence of the radiation field (photo-excitation) which is important for low-Z ions. We refer to Ness et al. (2000) for additional details. For O, the $G_{\rm obs}$ value corresponds to $T_e \approx 2.4$ MK. At this temperature, $R_{\rm obs}$ corresponds to a low density limit of 2×10^9 cm^{-3}. For Mg, the derived density is $n_e \approx 10^{12}$ cm^{-3} for a temperature close to the EM peak between 5–8 MK.

Dielectronic recombination (DR) satellite lines of He-like spectral lines in hot collisional plasmas are excellent additional indicators of the cool plasma temperature. Using the HULLAC code (Bar-Shalom et al. 1998), we have calculated the emitted spectrum of the He-like lines of O VII including the O VI DR satellite lines in the low-density limit. All of the 1snl and 1s2$ln'l'$ ($n' = 2$ to 4) levels are included in the computations. The resulting theoretical O spectra, as a function of electron temperature, are depicted in Fig 3 together with the data. The strongest DR satellites are at 22.02 Å and at 22.11 Å (Gabriel 1972). The bottom plot (0.02 keV) in the figure clearly demonstrates how at low temperature, the DR satellites dominate the spectrum. At slightly higher temperatures (0.05 keV), the higher lying satellites, in particular 1s2$l3l'$, produce relatively strong lines at 21.70 Å and at 21.63 Å, but eventually, as the temperature increases, the DR lines become weak and the He-like triplet lines prevail. The RGS data do not allow the identification of DR satellite lines, setting a lower limit of ≈ 1.2 MK to the cool plasma temperature.

In the case of the cool O triplet, both the line ratio and the DR satellite line approaches are consistent with the cool plasma temperature of the multi-T fits, and with the structure in the continuous DEM below 3 MK. However, the Mg triplet appears to be formed preferentially in the hot plasma around 7 MK.

5. Conclusions

The high-resolution X-ray spectrum of the binary star Capella, as observed by the RGS instruments, shows a multitude of transition lines from various elements such as Fe, Si, Mg, Ne, O, N, C, Ca, Ar, S. The derived elemental abundances are found to be generally below their solar photospheric values, or close to them. The high-FIP Ne is at about 0.4–0.5, consistent with previous suggestions from *ASCA* spectra (Brickhouse et al. 2000). While *ASCA* was not able to constrain the O abundance (Brickhouse et al. 2000), the RGS finds an abundance close the Ne abundance. C and N abundances appear to be 0.5 and ≈ 1 times their solar photospheric abundances, respectively. Other

elemental abundances are derived, although they principally emit weak L-shell lines in the RGS band. Furthermore, atomic code uncertainties for metallic L-shell lines caution us against overinterpreting the derived abundances. A realization of the DEM (Fig. 2) shows that it is continuous and that a sharp peak is found between 5–8 MK. Such a peak was suggested from previous *EUVE* data (Dupree et al. 1993) and recent *Chandra* LETG data (Mewe et al. 2000b), and HETG data (Behar et al. 2000). However, Canizares et al. (2000) derived a broad DEM from their HETG data. In our DEM, another peak at lower temperatures (1.2–2.5 MK) is found, albeit with a lower EM. This bump is mainly required in order to account for the bright emission lines from the cool O VII triplet and C VI Lyα. Densities from the cool O VII and hot Mg XI triplets appear to differ by three orders of magnitude, the first indicating $\approx 10^9$ cm^{-3}, consistent with previous LETG results (Brinkman et al. 2000, Ness et al. 2000) but lower than for the HETG (Canizares et al. 2000), and the second indicating $\approx 10^{12}$ cm^{-3}. Dupree et al. (1993) derived an electron density from the hot Fe XXI which is compatible with the density derived here for Mg. HETG data suggested a high density for hotter plasma for the Mg triplet as well (Canizares et al. 2000).

It appears, then, that the coronae of Capella are bi-modal: On the one hand, we find low-density cool plasma, and on the other hand, we measure high densities for hot plasma. Because it is likely that there is a broad distribution of electron density in the coronae of Capella, we cannot exclude the presence of cool high-density and hot low-density material. However, it is probable that the two detected plasma portions belong to distinct and different features in the stellar coronae, given the magnitude of their density and temperatures differences.

The high-resolution, high signal-to-noise X-ray spectrum of Capella measured by the RGS instrument on board the *XMM-Newton* satellite offers unprecedented insight into deficiencies in the present atomic codes. We have shown that a number of lines can influence the derivation of elemental abundances, especially if no K-shell lines (which are in general well-described in the codes) are present in the data. Metallic L-shell ions are typically ill-described in the current fitting codes (MEKAL, SPEX) used in the astronomical community. However, their usual intensity is low compared to the bright K-shell lines. Although the high-resolution spectra from *XMM-Newton* and *Chandra* provide direct evidence of inconsistencies in the atomic codes, the overall agreement of the model with the dominant lines suggests that previous low-resolution CCD spectral fitting results with a global approach are not invalidated. The X-ray spectra collected from the new generation of X-ray satellites will put strong constraints on existing codes.

Acknowledgements. M. A. acknowledges support from the Swiss National Science Foundation, grant 21-49343.96, from the Swiss Academy of Sciences and from the Swiss Commission for Space Reasearch. The Space Research Organization Netherlands (SRON) is supported financially by NWO.

References

Bar-Shalom A., Klapisch M., Goldstein W. H., Oreg J., 1998, *The HULLAC code for atomic physics*, (unpublished)
Behar E., Cottam J., Kahn S. M., 2000, astro-ph/0003099
Brickhouse N. S., Dupree A. K., Edgar R. J., Liedahl D. A., Drake S. A., White N. E., Singh K. P., 2000, ApJ 530, 387
Brinkman A. C., Gunsing C. J. T., Kaastra J. S., et al., 2000, ApJ 530, L111
Brown G. V., Beiersdorfer P., Liedahl D. A., Widmann K., Kahn S. M., 1998, ApJ 502, 1015
Canizares C. R., Huenemoerder D. P., Davis D. S., et al., 2000, ApJ 539, L41
Cash W., Bowyer S., Charles P. A., Lampton M., Garmire G., Riegler G., 1978, ApJ 223, L21
Catura R. C., Acton L. W., Johnson H. M., 1975, ApJ 196, L47
Dupree A. K., Brickhouse N. S., Doschek G. A., Green J. C., Raymond J. C., 1993, ApJ 418, L41
Favata F., Mewe R., Brickhouse N. S., Pallavicini R., Micela G., Dupree A. K., 1997, A&A 324, L37
Gabriel A. H., 1972 MNRAS 160, 99
Gabriel A. H, Jordan C., 1969, MNRAS 145, 241
den Herder J. W., et al., 2000, A&A, this issue
Holt S. S., White N. E., Becker R. H., et al., 1979, ApJ 234, L65
Hummel C. A., Armstrong J. T., Quirrenbach A., Buscher D. F., Mozurkewich D., Elias II N. M., 1994, AJ 107, 1859
Jansen F., et al., 2000, A&A, this issue
Kaastra J. S., Mewe R., Nieuwenhuijzen H., 1996, In: Yamashita K., Watanabe T. (eds.) UV and X-ray Spectroscopy of Astrophysical and Laboratory Plasmas. Univ. Acad. Press, Tokyo, p. 411
Lemen J. R., Mewe R., Schrijver C. J., Fludra A., 1989, ApJ 341, 474
Linsky J. L, Brown A., Gayley K., et al., 1993, ApJ 402, 694
Linsky J. L., Wood B.E., Brown A., Osten R. A., 1998, ApJ 492, 767
Mason K., et al., 2000, A&A, this issue
Mewe R., Gronenschild E. H. B. M., Westergaard N. J., et al., 1982 260, 233
Mewe R., Heise J., Gronenschild E. H. B. M., Brinkman A. C., Schrijver J., den Boggende A. J. F., 1975, ApJ 202, L67
Mewe R., Kaastra J. S., Liedahl D. A., 1995, Legacy 6, 16
Mewe R., Porquet D., Raassen A. J. J., Kaastra J. S., Dubau J., 2000, (in preparation)
Mewe R., Raassen A. J. J., Drake J. J., Kaastra J. S., van der Meer R. L.J., 2000, (in preparation)
Ness J. U., Mewe R., Schmitt J. H. M. M., Raassen A. J. J., Porquet D., et al., 2000, A&A, (submitted)
Perryman M. A. C., et al., 1997, A&A 323, L49
Phillips K. J. H., Mewe R., Harra-Murnion L. K., Kaastra J. S., Beiersdorfer P., Brown G. V., Liedahl D. A., 1999, A&AS 138, 381
Porquet D., Dubau, J., 2000, A&AS 143, 495
Pradhan A. K., 1982, ApJ 263, 477
Schrijver C. J., Mewe R., van den Oord G. H. J., Kaastra J. S., 1995, A&A 302, 438
Strassmeier K. G., Fekel F. C., 1990, A&A 230, 389
Strüder L., et al., 2000, A&A, this issue
Turner M. J. L., et al., 2000, A&A, this issue
Vedder P. W., Canizares C. R., 1983, ApJ 270, 666